Journal of the Optical Society of America A
OPTICS, IMAGE SCIENCE, AND VISION

Dynamics of accelerating Bessel solutions of Maxwell's equations

Parinaz Aleahmad,[1] Hector Moya Cessa,[2] Ido Kaminer,[3] Mordechai Segev,[4] and Demetrios N. Christodoulides[1,*]

[1]CREOL, College of Optics and Photonics, University of Central Florida, Orlando, Florida 32816-2700, USA
[2]INAOE, Coordinacion de Optica, Luis Enrique Erro No.1, 72840 Tonantzintla, Puebla, Mexico
[3]Department of Physics, Massachusetts Institute of Technology, 77 Massachusetts Avenue, Cambridge, Massachusetts 02139, USA
[4]Physics Department and Solid State Institute, Technion-Israel Institute of Technology, Haifa 32000, Israel
*Corresponding author: demetri@creol.ucf.edu

Received 6 July 2016; revised 15 August 2016; accepted 28 August 2016; posted 29 August 2016 (Doc. ID 269793); published 22 September 2016

We investigate the propagation dynamics of accelerating beams that are shape-preserving solutions of the Maxwell equations, and explore the contribution of their evanescent field components in detail. Both apodized and non-apodized Bessel beam configurations are considered. We show that, in spite of the fact that their evanescent tails do not propagate, these nonparaxial beams can still accelerate along circular trajectories and can exhibit large deflections. Subsequently, our formulation is extended in other two-dimensional vectorial arrangements. The reported results can be useful in plasmonic and other subwavelength and near-field settings.

OCIS codes: (050.1960) Diffraction theory; (070.7345) Wave propagation.

http://dx.doi.org/10.1364/JOSAA.33.002047

1. INTRODUCTION

In 2007, the concept of accelerating beams was first introduced in optics through a new class of diffraction-free waves, the so-called Airy beams [1,2]. First conceived within the context of quantum mechanics [3], these self-similar Airy wave packets are known to exhibit some very remarkable properties. Perhaps the most intriguing of them is their very ability to freely accelerate. Interestingly, in optics, this latter property takes on a whole new meaning. It implies that the intensity features of an Airy beam can self-bend even in an entirely homogeneous media-like vacuum, etc. In this case, an Airy beam can accelerate along a parabolic trajectory, very much like a projectile moving under the action of gravity. Over the last few years, optical Airy beams have found applications in many and diverse settings. These range from inducing curved plasma filaments in air and autofocusing collapse [4–7], to extending the supercontinuum generation in photonic crystal fibers [8] and producing spatiotemporal light bullets that are impervious to both dispersion and diffraction effects [9,10]. Airy wave packets represent the only nondiffracting solution in 1D, and as such, they could be potentially useful in realizing self-bending surfaces and interfaces, such as plasmons [11–13]. In addition to their aforementioned characteristics, these wavefronts also happen to be self-healing—an advantageous property in adverse environments where scattering is an issue [14]. Along these lines, Airy beams have been successfully used in manipulating microparticles [15] and quite recently in STORM microscopies [16]. Strategies for micromachining surfaces have been introduced [17], and the use of similar schemes in producing electron Airy packets has been pursued. Finally, the prospect of using nonlinearities in conjunction with such accelerating waves has been studied [18–21].

As previously indicated, the Airy wave function represents the only accelerating solution (in 1D) to the paraxial equation of diffraction. Clearly of interest would be to extend these concepts into the nonparaxial domain, associated with near-field applications. Lately, a new family of nonparaxial accelerating wave packets was presented by considering the vectorial Bessel solutions of the Helmholtz equation in cylindrical coordinates [22]. Shortly after, nonparaxial accelerating beams were experimentally observed [23], and within a few months, accelerating nonparaxial beams were also found in the nonlinear domain [24,25]. In general, Bessel accelerating waves can move on a circular trajectory with a radius of only a few wavelengths. Subsequently, other classes of nonparaxial accelerating wave packets have been suggested and observed [26–29]. These include, for example, Mathieu and Weber beams that follow elliptic and parabolic trajectories, respectively, as well as 3D fully vectorial wave packets in the form of spherical Bessel and oblate/prolate spheroidal functions [26,29–31]. Very recently, these 3D nonparaxial accelerating wave packets were observed in a series of experiments [32]. In addition,

Corrected 22 September 2016

self-accelerating Bessel-like beams were generated experimentally from multimode fiber arrangements [33], and generalized radially self-accelerating Helicon waves were produced using spatial light modulators and theoretically investigated [34]. Finally, the dynamics of nonparaxial accelerating Bessel beams shifting laterally along fairly arbitrary trajectories were considered based on stationary phase methods and the underlying ray dynamics [35].

It is important to emphasize that the aforementioned accelerating wavefronts are solutions to the full-vector Maxwell equations in coordinate systems where the vectorial Helmholtz problem can be successfully separated. In fact, they correspond to modes in cavity configurations, when the enclosing "perfect metallic boundary" is eventually pushed to infinity. For instance, the Bessel waves (TE or TM) happen to be the circulating modes in a cylindrical cavity, of infinite extent. As a result, when this solution is launched from a single input plane in free space, it tends to self-bend along a circular trajectory, as in a cavity, until the open boundary conditions take a toll. Given that these are highly nonparaxial solutions, it will be of importance to understand the role of evanescent contributions on their propagation. In addition, at this point, it is not very clear how these beams will dynamically evolve even if they are not truncated. In other words, how will they propagate if the entire waveform (that in principle extends to infinity) is provided? These questions can only be answered through an exact analytical approach, since any numerical attempt has to rely on apodized versions of such beams.

In this paper, we present close-form analytic results describing the evolution of accelerating solutions of the full Maxwell equations. We analyze the specific case of such beams that accelerate along circular trajectories, for which the analytic solutions correspond to the Bessel functions—when the beams are not truncated [24]. The contribution of the evanescent field components on the propagation of these vectorial wave packets is investigated in detail. We show that, in spite of evanescent components, these nonparaxial beams can still accelerate up to a point, along circular trajectories, and in doing so they can exhibit large deflections. Both apodized and nonapodized Bessel beam configurations are considered. This formulation is then extended in other two-dimensional vectorial arrangements.

2. PROPAGATION DYNAMICS OF SEMI-INFINITE BESSEL BEAMS

We begin our analysis by considering the Helmholtz equation in two dimensions $(\nabla^2 + k^2)\{\vec{E}, \vec{H}\} = 0$, where $k = \omega n/c$ represents the wavenumber. Without any loss of generality, we here assume a transverse-electric mode, i.e., $\vec{E} = E_y(x, z)\hat{y}$. When this problem is treated in cylindrical coordinates, the following circulating mode can be directly obtained in terms of Bessel functions:

$$\vec{E} = J_\nu(kr)e^{i\nu\phi}\hat{y}, \tag{1}$$

where $r = \sqrt{x^2 + z^2}$ and $\phi = \tan^{-1}(z/x)$. From Maxwell's equations one can then deduce the magnetic field components, i.e., $H_x = (\mu_0\omega)^{-1}e^{i\nu\phi}\{iJ'_\nu(kr)kz/r - J_\nu(kr)\nu x/r^2\}$ and $H_z = -(\mu_0\omega)^{-1}e^{i\nu\phi}\{iJ'_\nu(kr)kx/r + J_\nu(kr)\nu z/r^2\}$, where derivatives are given with respect to the argument of the Bessel function. The diffraction behavior of this nonparaxial Bessel beam is then investigated in the vectorial Helmholtz regime by means of a Fourier integral, i.e.,

$$E_y(x, z) = \frac{1}{2\pi}\int_{-\infty}^{\infty} \mathrm{d}\omega F(\omega)e^{i\omega x}e^{iz\sqrt{k^2-\omega^2}}, \tag{2}$$

where z is the propagation direction and $F(\omega) = \int_{-\infty}^{\infty} E_y(x, 0)e^{-i\omega x}\mathrm{d}x$, represents the Fourier spectrum of the electric field at $z = 0$. In Eq. (2) ω stands for the transverse wave vector k_x.

In what follows, we examine the dynamical evolution of a half-branch Bessel wave packet—typically used in experimental arrangements. In this case, $E_y(x, 0) = H(x)J_\nu(kx)$, where $H(x)$ represents a Heaviside step function. As we will see, this abrupt step-apodization will introduce evanescent contributions that play an important role in the ensuing diffraction dynamics. For a semi-infinite Bessel function of the form $J_\nu(kx)$, associated with an angular number ν, $F(\omega)$ can be obtained from the respective sine and cosine Fourier transforms (defined in the interval $[0, \infty]$) which are given by [36],

$$F_c(\omega) = (k^2 - \omega^2)^{-\frac{1}{2}}\cos\left\{\nu\sin^{-1}\left(\frac{\omega}{k}\right)\right\}, \qquad \omega < k \tag{3a}$$

$$F_c(\omega) = -k^\nu \sin\left(\frac{\nu\pi}{2}\right)(\omega^2 - k^2)^{-\frac{1}{2}}\left\{\omega + (\omega^2 - k^2)^{\frac{1}{2}}\right\}^{-\nu}, \quad \omega > k \tag{3b}$$

$$F_s(\omega) = (k^2 - \omega^2)^{-\frac{1}{2}}\sin\left\{\nu\sin^{-1}\left(\frac{\omega}{k}\right)\right\}, \quad \omega < k \tag{3c}$$

$$F_s(\omega) = k^\nu \cos\left(\frac{\nu\pi}{2}\right)(\omega^2 - k^2)^{-\frac{1}{2}}\left\{\omega + (\omega^2 - k^2)^{\frac{1}{2}}\right\}^{-\nu}, \quad \omega > k. \tag{3d}$$

Here $F_c(\omega) = \int_0^\infty J_\nu(kx)\cos(\omega x)\mathrm{d}x$ and $F_s(\omega) = \int_0^\infty J_\nu(kx)\sin(\omega x)\mathrm{d}x$. By writing the Fourier transform in Eq. (2), in terms of a sine (odd) and a cosine (even) Fourier component, i.e., $F(\omega) = e(\omega) - io(\omega)$, and by rewriting the oscillating exponential as $e^{i\omega x} = \cos(\omega x) + i\sin(\omega x)$, the integral in Eq. (2) assumes the form

$$E_y(x, z) = \frac{1}{2\pi}\int_{-\infty}^{\infty} \mathrm{d}\omega[e(\omega)\cos(\omega) + o(\omega)\sin(\omega x)]e^{iz\sqrt{k^2-\omega^2}}. \tag{4}$$

Because of the symmetry properties of Eq. (3), it is more convenient to study the cases of even and odd Bessel orders separately.

We first consider the propagating component [where $-k \le \omega \le k$ in Eq. (4)] from even-order Bessel functions ($\nu = 2m$). By using $\omega = k\sin\theta$, the integral related to the cosine contribution E_y^c takes the form

$$E_y^c(x, z) = \frac{1}{2\pi}\int_{-\frac{\pi}{2}}^{\frac{\pi}{2}} \mathrm{d}\theta\cos(2m\theta)e^{ikx\sin\theta}e^{izk\cos\theta}. \tag{5}$$

For convenience, we define a new variable as $\phi = \sin^{-1}(z/r)$, so the integral in Eq. (5) becomes

$$E_y^c(x, z) = \frac{1}{2\pi}\int_{-\frac{\pi}{2}}^{\frac{\pi}{2}} \mathrm{d}\theta\cos(2m\theta)e^{ikr\sin(\theta+\phi)}. \tag{6}$$

By expanding the exponential component in terms of Bessel functions, $e^{ix\sin\theta}=\sum_{n=-\infty}^{\infty}e^{in\theta}J_n(x)$ [37], and by changing the order of integration with the summation, one can get an exact closed form solution to the integral in Eq. (6),

$$E_y^c(x,z)=\frac{1}{2}\cos(2m\phi)J_{2m}(kr),+\frac{i}{\pi}(-1)^m\sum_{n=0}^{\infty}(-1)^nJ_{2n+1}(kr)\sin[(2n+1)\phi]\times\frac{4n+2}{(2n+1)^2-4m^2}. \tag{7}$$

A similar procedure can be followed to obtain the propagating field component ($|\omega|\le k$) from the sine part, E_y^s in Eq. (4) which is given by

$$E_y^s(x,z)=\frac{-1}{2}\sin(2m\phi)J_{2m}(kr),+\frac{i}{\pi}(-1)^m\sum_{n=0}^{\infty}(-1)^nJ_{2n+1}(kr)\cos[(2n+1)\phi]\times\frac{4m}{(2n+1)^2-4m^2}. \tag{8}$$

For and even-order semi-infinite Bessel accelerating beam, it is clear from Eq. (3) that the evanescent contribution comes only from the odd part [Eq. (3d)] in the integral of Eq. (4). In this case ($\nu=2m$) after substituting Eq. (3d) in Eq. (4) and after writing $\omega=k\cosh\theta$, the integral for the evanescent part reads as follows:

$$E_y(x,z)=\frac{(-1)^m}{\pi}\mathrm{Im}\left[\int_0^{\infty}d\theta e^{ikx\cosh\theta}e^{-zk\sinh\theta}e^{-2m\theta}\right]\quad(\omega>k). \tag{9}$$

The dominant contribution to the integral comes mainly from the region $\theta\approx 0$, since the integrant oscillates very fast outside the aforementioned range and hence cancels out. In this case, one can use the approximation $\sinh\theta\sim\theta$ and $\cosh\theta\sim 1+\theta^2/2$. As a result, the evanescent integral can be obtained; hence,

$$E_y(x,z)=\frac{(-1)^m}{\pi}\mathrm{Im}\times\left[e^{ikx}\sqrt{\frac{i\pi}{2kx}}e^{\frac{i}{2kx}(zk+2m)^2}\left(1-\mathrm{erf}\left(\frac{zk+2m}{\sqrt{-2ikx}}\right)\right)\right]\quad(\omega>k). \tag{10}$$

By combining the above results, one finds that the propagation dynamics of a half-even Bessel function ($\nu=2m$) is given by

$$E_y(x,z)=\frac{1}{2}J_{2m}(kr)e^{2im\phi}+\frac{i}{\pi}(-1)^m\sum_{n=0}^{\infty}(-1)^nJ_{2n+1}(kr)\times\left[\sin[(2n+1)\phi]\frac{4n+2}{(2n+1)^2-4m^2}-i\cos[(2n+1)\phi]\frac{4m}{(2n+1)^2-4m^2}\right]+\frac{(-1)^m}{\pi}\mathrm{Im}\times\left[e^{ikx}\sqrt{\frac{i\pi}{2kx}}e^{\frac{i}{2kx}(zk+2m)^2}\left(1-\mathrm{erf}\left(\frac{zk+2m}{\sqrt{-2ikx}}\right)\right)\right]. \tag{11}$$

A similar theoretical analysis can be carried out for an odd-order Bessel function when $E_y(x,0)=H(x)J_{2m+1}(kx)$. In this case, the odd part of the Fourier transform is proportional to $\sin(m\pi)$ in the range ($\omega>k$) and is therefore zero. As a result, any evanescent contribution arises from the even component [Eq. (3b)]. From here, one obtains an expression for the diffraction dynamics of an odd-order semi-infinite accelerating Bessel beam:

$$E_y(x,z)=\frac{1}{2}J_{2m+1}(kr)e^{i(2m+1)\phi}+\frac{(-1)^m}{\pi}\sum_{n=1}^{\infty}(-1)^nJ_{2n}(kr)\times\left[\cos(2n\phi)\frac{4m+2}{(2m+1)^2-4n^2}+i\sin(2n\phi)\frac{4n}{(2m+1)^2-4n^2}\right]+\frac{(-1)^{m+1}}{\pi}\mathrm{Re}\left[e^{ikx}\sqrt{\frac{i\pi}{2kx}}e^{\frac{i}{2kx}(zk+2m+1)^2}\times\left(1-\mathrm{erf}\left(\frac{zk+2m+1}{\sqrt{-2ikx}}\right)\right)\right], \tag{12}$$

where again the last part of Eq. (12) describes evanescent contributions during propagation. Figures 1(a) and 1(b) show two-dimensional intensity patterns for the case of accelerating half-even Bessel wave packets, as obtained from Eq. (11), when $2m=10$ and $2m=50$, respectively. The validity of the approximations used to obtain the evanescent components was also checked numerically. It is clear from Eqs. (11) and (12) and from Figs. 1(a) and 1(b) that, in spite of the fact that the semi-infinite Bessel beam is by no means apodized (i.e., all the lobes have been provided in the initial field distribution on the semi-infinite x-axis), the beam eventually diffracts after a certain propagation distance. This is caused by all the higher-order terms (including the evanescent) in Eqs. (11) and (12). Clearly the beam accelerates or self-bends to a great extent before diffraction effects take a toll. For example, if $2m=10$, the beam reaches a deflection of 25° while for $2m=50$, the self-bending is approximately 50°. Figures 1(c) and 1(d) show the intensity variation of the main lobe as a function of the angle of propagation for $2m=10$ and $2m=50$, respectively. Evidently, the higher-order Bessel beams tend to

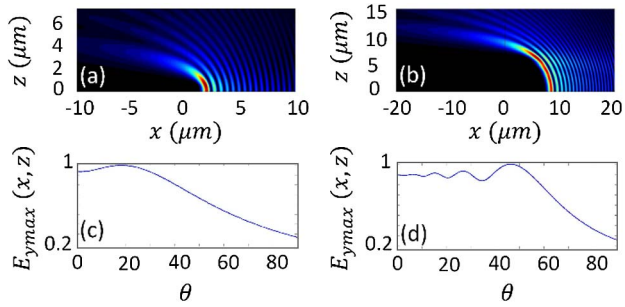

Fig. 1. Intensity profile of a propagating even-order half-Bessel wave packet when launched from the x-axis, for (a) $2m=10$, and (b) $2m=50$. (c, d) Normalized intensity variation of the main lobe as a function of the propagation angle, corresponding to the propagation dynamics shown in (a, b), respectively. In plotting these results the first 30 terms in Eq. (11) were used.

experience more oscillations during propagation, as the evanescent field contribution fades out faster. To some extent, this is because the Bessel beam realized is no longer a circulating mode in perfect cylindrical metallic cavity and hence gradually tends to disintegrate. In other words, the half-Bessel beam is not a natural mode of the free-space Helmholtz problem. In addition, one can show that for higher-order Bessel functions, the bending radius increases asymptotically according to the relation $r \sim \lambda/2\pi[\nu + 0.808\nu^{1/3} + 0.072\nu^{-1/3}]$, where ν stands for the order of the Bessel function. As a result, the beam-envelope will follow a longer path for higher-orders and the evanescent part plays little role during propagation. This effect can be seen in Eqs. (10) and (12), where the argument of the error function increases with ν. Moreover, for large orders, the width of the first lobe can be approximated by $\Delta \sim \lambda/2\pi[2.094\nu^{1/3} + 1.921\nu^{-1/3}]$. Similar results can be obtained for nonparaxial odd-order half-Bessel beams.

3. PROPAGATION DYNAMICS OF HALF-BRANCH APODIZED BESSEL BEAMS

As was mentioned before, all the optical diffraction-free arrangements possess an infinite norm. Hence, it is often necessary to apodize them in order to observe them experimentally. As one could expect, this apodization can effectively influence their propagation. To investigate these effects, we consider the diffraction behavior of an apodized version of such accelerating Bessel beams. Here we choose the apodization function to be $1/x$, ensuring that the wave packet has a finite energy. As we will see, this particular apodization leads to closed form solutions for both propagating and evanescent contributions. In this case, the launched field follows $E_y(x, 0) = J_\nu(kx)/x$, as defined in the interval $x \geq 0$ (apodized half-branch Bessel beam). By using the equation $J_\nu(kx)/x = 1/2\nu[J_{\nu-1}(kx) + J_{\nu+1}(kx)]$ and the results from the previous section, the propagation dynamics of such apodized even-order Bessel beams ($\nu = 2m$), can be expressed as follows:

$$
\begin{aligned}
E_y(x,z) = {} & \frac{1}{8m}[J_{2m+1}(kr)e^{i(2m+1)\phi} + J_{2m-1}(kr)e^{i(2m-1)\phi}] \\
& + \frac{(-1)^m}{4m\pi}\sum_{n=1}^{\infty}(-1)^n J_{2n}(kr) \\
& \times \left\{ \cos(2n\phi)\left[\frac{4m+2}{(2m+1)^2-4n^2} + \frac{-4m+2}{(2m-1)^2-4n^2}\right] \right. \\
& \left. + i\sin(2n\phi)\left[\frac{4n}{(2m+1)^2-4n^2} + \frac{-4n}{(2m-1)^2-4n^2}\right]\right\} \\
& + \frac{(-1)^{m+1}}{4m\pi}\,\mathrm{Re}\left[e^{ikx}\sqrt{\frac{i\pi}{2kx}}e^{\frac{i}{2kx}(zk+2m+1)^2}\right. \\
& \left. \times\left(1 - \mathrm{erf}\left(\frac{zk+2m+1}{\sqrt{-2ikx}}\right)\right)\right] \\
& + \frac{(-1)^m}{4m\pi}\,\mathrm{Re}\left[e^{ikx}\sqrt{\frac{i\pi}{2kx}}e^{\frac{i}{2kx}(zk+2m-1)^2}\right. \\
& \left. \times\left(1 - \mathrm{erf}\left(\frac{zk+2m-1}{\sqrt{-2ikx}}\right)\right)\right]. \qquad (13)
\end{aligned}
$$

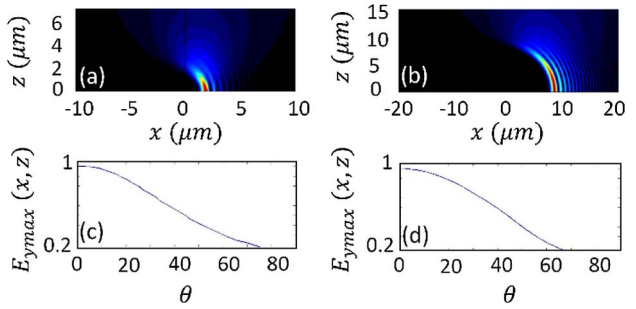

Fig. 2. Intensity distribution of a propagating even-order half-Bessel apodized wave packet when launched from the x-axis for (a) $2m = 10$, and (b) $2m = 50$. (c, d) Normalized intensity variation of the first lobe with respect to the angle of propagation, corresponding to the patterns shown in (a, b), respectively.

Again, all the terms associated with the complex error functions describe evanescent field contributions. Figure 2 depicts plots of these analytical results as obtained from Eq. (13) for two different orders, $\nu = 10$ and $\nu = 50$. In all cases, the nonparaxial acceleration behavior is evident in spite of the apodization. The validity of the approximations used to obtain the evanescent components was also checked numerically. Note that in this case, the intensity of the main lobe is oscillation-free due to the apodization. Similar results can be obtained for $1/x$ apodized odd-order half-Bessel beams.

4. DYNAMICAL EVOLUTION OF FULLY SYMMETRIC ACCELERATING BESSEL BEAMS

Interestingly, Bessel wave packets taken on the entire x-axis (full Bessel beams) lack evanescent contributions irrespective of whether they are even or odd. This is a direct result of symmetry in conjunction with Eq. (3). As an example, for an even-order Bessel function with initial distribution $E_y(x, 0) = J_\nu(kx)$, where $\nu = 2m$ with m being an integer, the sine contributions to the Fourier transform cancel out due to spatial symmetry. Moreover, as it is clear in Eq. (3b), the evanescent part ($\omega > k$) would be proportional to $\sin(m\pi)$, which is absent. Hence by substituting the only remaining term from Eq. (3a), the integral in Eq. (2) (after a change of variable $\omega = k \sin\theta$) assumes the form

$$E_y(x,z) = \frac{1}{\pi}\int_{-\frac{\pi}{2}}^{\frac{\pi}{2}} \mathrm{d}\theta\, \cos(2m\theta)e^{ikx\sin\theta}e^{izk\cos\theta}. \qquad (14)$$

To evaluate the integral in Eq. (14), a similar approach to the one described before is followed. However, it is important to stress that this time, only the cosine part of the Fourier transform contributes to the propagation. One can get an exact closed form solution to the integral in Eq. (14):

$$
\begin{aligned}
E_y(x,z) = {} & \cos(2m\phi)J_{2m}(kr), \\
& + \frac{2i}{\pi}(-1)^m\sum_{n=0}^{\infty}(-1)^n J_{2n+1}(kr) \\
& \times \sin[(2n+1)\phi]\frac{4n+2}{(2n+1)^2-4m^2}. \qquad (15)
\end{aligned}
$$

Equation (15) describes the acceleration pattern of an even-Bessel function in free space. The first term in this equation

ensures that the initial Bessel function is present in the intensity pattern during evolution. However, the rest of the terms introduce variations in the initial distribution. A similar result can be obtained when, $\nu = 2m + 1$, for odd-order Bessel functions. Following the same procedure described before, one can get a similar result to Eq. (15) for the propagation pattern of an entire odd-order Bessel function:

$$E_y(x,z) = \cos[(2m+1)\phi]J_{2m+1}(kr), + \frac{2i}{\pi}(-1)^m \sum_{n=1}^{\infty}(-1)^n J_{2n}(kr)\sin[(2n)\phi] \times \frac{4n}{(2m+1)^2 - 4n^2}. \quad (16)$$

As in the previous case, the initial field configuration persists during propagation and asymptotically follows a semicircular path. Figures 3(a) and 3(b) show two-dimensional plots corresponding to the intensity profile of an even/odd order Bessel distribution as described by Eqs. (15) and (16), when $m = 25$. As is clear from Fig. 3, interference effects take place in both the left and right branches, even after a short distance of propagation—even before the two branches collide. Note that this change affects the lobes, while the intensity profile of the semicircle remains unchanged, and as a result, the acceleration trajectory remains circular. As Fig. 3 shows, this interference pattern can lead to a constructive focusing of these two branches; thus a maximum is attained on the z-axis for an even-order Bessel function. Conversely, the intensity is zero on the z-axis for the odd case due to destructive interference.

5. VECTORIAL BESSEL WAVE PACKETS

In principle, we can extend this treatment in three dimensions. To establish such beams, one should treat Maxwell's equations

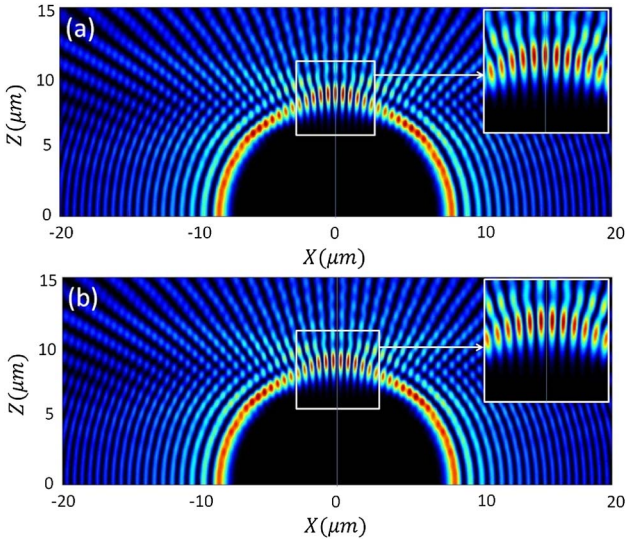

Fig. 3. Intensity profile of a full-Bessel beam when propagating toward the z-axis for (a) an even-order symmetric Bessel field distribution when $2m = 50$, and (b) an odd-order antisymmetric Bessel distribution with $2m + 1 = 51$. The corresponding interference patterns resulting from these initial conditions are highlighted in the insets.

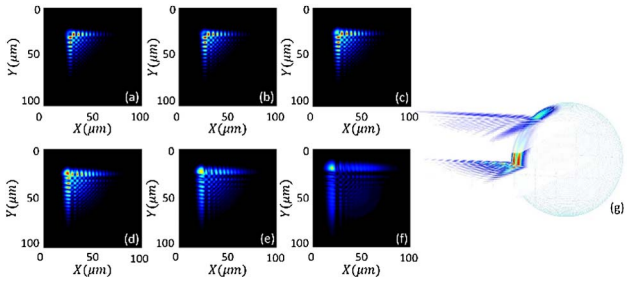

Fig. 4. Two-dimensional cross section of the intensity profile associated with a 3D vectorial Bessel accelerating beam propagating in free space with $\alpha = \beta = 1$ and $m = n = 25$, when (a) $z = 0$, (b) $z = 4$ (c) $z = 8$, (d) $z = 12$, (e) $z = 16$, (f) $z = 24$ μm. (g) To demonstrate the acceleration effect, the propagation of the main lobe is mapped on a spherical surface.

in the vectorial domain. Here we assume that at the excitation plane $z = 0$, the field distribution has a separable form in terms of two functions, f and g:

$$E(x,y,0) = \hat{x}f(x)G(y) + \hat{y}F(x)g(y), \quad (17)$$

where $G(y) = dg(y)/dy$ and $F(x) = -df(x)/dx)$. Starting from the Helmholtz equation, one can then show that the electric field evolves with z, as follows:

$$E(x,y,z) = \frac{1}{(2\pi)^2}\iint_{-\infty}^{\infty} \mathrm{d}k_x \mathrm{d}k_y \mathcal{F}(k_x) \times \mathcal{G}(k_y)[ik_y\hat{x} - ik_x\hat{y}]e^{i(k_x x + k_y y)}e^{iz\sqrt{k^2 - k_x^2 - k_y^2}}, \quad (18)$$

where $\mathcal{F}(k_x)$ and $\mathcal{G}(k_y)$ represent the Fourier transforms of $f(x)$ and $g(y)$, respectively. Note that everywhere Eq. (18) satisfies $\nabla \cdot \vec{E} = 0$. From here, the magnetic field corresponding to Eq. (18) can be obtained. In order to establish an accelerating Bessel beam in 2D, here we assume semi-infinite Bessel functions, $f(x) = J_m(\alpha x)$ and $g(y) = J_n(\beta y)$, where α and β are real numbers. Since in general the two Bessel functions have different orders and different arguments, such a solution has the flexibility of accelerating along the x and y directions at different rates. The propagation dynamics of this double-Bessel solution is illustrated in Fig. 4, where the evolution of the beam cross sections in the x–y plane is depicted for different values of z. In this figure, we have used Bessel functions with orders $m = n = 25$ and $\alpha = \beta = 1$. As Fig. 4 clearly indicates, the double-Bessel beam accelerates along both x and y axes, asymptotically reaching the center of the coordinate system after a certain distance of propagation. To better visualize these dynamics, we have also mapped the propagation of the main lobe of this Bessel–Bessel accelerating beam on the surface of a sphere [Fig. 4(g)].

6. DISCUSSION AND CONCLUSIONS

We have investigated the dynamics of accelerating Bessel wave packets following circular trajectories in free space. We have presented analytical results for the evolution of Bessel-beams in 2D, and we showed that the acceleration behavior can persist even in the presence of evanescent components. Our results

could be of relevance in microparticle manipulation [38,39] and other subwavelength settings.

Funding. United States-Israel Binational Science Foundation (BSF) (2010138); Israeli Ministry of Defense (4440335493).

REFERENCES

1. G. A. Siviloglou and D. N. Christodoulides, "Accelerating finite energy Airy beams," Opt. Lett. **32**, 979–981 (2007).
2. G. A. Siviloglou, J. Broky, A. Dogariu, and D. N. Christodoulides, "Observation of accelerating Airy beams," Phys. Rev. Lett. **99**, 213901 (2007).
3. M. V. Berry and N. L. Balazs, "Nonspreading wave packets," Am. J. Phys. **47**, 264–267 (1979).
4. P. Polynkin, M. Kolesik, J. V. Moloney, G. A. Siviloglou, and D. N. Christodoulides, "Curved plasma channel generation using ultraintense Airy beams," Science **324**, 229–232 (2009).
5. N. K. Efremidis and D. N. Christodoulides, "Abruptly autofocusing waves," Opt. Lett. **35**, 4045–4047 (2010).
6. D. G. Papazoglou, N. K. Efremidis, D. N. Christodoulides, and S. Tzortzakis, "Observation of abruptly autofocusing waves," Opt. Lett. **36**, 1842–1844 (2011).
7. P. Zhang, J. Prakash, Z. Zhang, M. S. Mills, N. K. Efremidis, D. N. Christodoulides, and Z. Chen, "Trapping and guiding microparticles with morphing autofocusing Airy beams," Opt. Lett. **36**, 2883–2885 (2011).
8. C. Ament, P. Polynkin, and J. V. Moloney, "Supercontinuum generation with femtosecond self-healing Airy pulses," Phys. Rev. Lett. **107**, 243901 (2011).
9. A. Chong, W. H. Renninger, D. N. Christodoulides, and F. W. Wise, "Airy-Bessel wave packets as versatile linear light bullets," Nat. Photonics **4**, 103–106 (2010).
10. D. Abdollahpour, S. Suntsov, D. G. Papazoglou, and S. Tzortzakis, "Spatiotemporal Airy light bullets in the linear and nonlinear regimes," Phys. Rev. Lett. **105**, 253901 (2010).
11. A. Salandrino and D. N. Christodoulides, "Airy plasmon: a nondiffracting surface wave," Opt. Lett. **35**, 2082–2084 (2010).
12. P. Zhang, S. Wang, Y. Liu, X. Yin, C. Lu, Z. Chen, and X. Zhang, "Plasmonic Airy beams with dynamically controlled trajectories," Opt. Lett. **36**, 3191–3193 (2011).
13. A. Minovich, A. E. Klein, N. Janunts, T. Pertsch, D. N. Neshev, and Y. S. Kivshar, "Generation and near-field imaging of Airy surface plasmons," Phys. Rev. Lett. **107**, 116802 (2011).
14. J. Broky, G. A. Siviloglou, A. Dogariu, and D. N. Christodoulides, "Self-healing properties of optical Airy beams," Opt. Express **16**, 12880–12891 (2008).
15. J. Baumgartl, M. Mazilu, and K. Dholakia, "Optically mediated particle clearing using Airy wavepackets," Nat. Photonics **2**, 675–678 (2008).
16. S. Jia, J. C. Vaughan, and X. Zhuang, "Isotropic 3D super-resolution imaging with a self-bending point spread function," in *Conference on Lasers and Electro-Optics (CLEO)*, California (Optical Society of America, 2013), paper CTh5D.10.
17. A. Mathis, L. Froehly, L. Furfaro, M. Jacquot, J. M. Dudley, and F. Courvoisier, "Direct machining of curved trenches in silicon with femtosecond accelerating beams," J. Eur. Opt. Soc. **8**, 13019 (2013).
18. T. Ellenbogen, N. Voloch-Bloch, A. Ganany-Padowicz, and A. Arie, "Nonlinear generation and manipulation of Airy beams," Nat. Photonics **3**, 395–398 (2009).
19. I. Kaminer, M. Segev, and D. N. Christodoulides, "Self-accelerating self-trapped optical beams," Phys. Rev. Lett. **106**, 213903 (2011).
20. I. Dolev, I. Kaminer, A. Shapira, M. Segev, and A. Arie, "Experimental observation of self-accelerating beams in quadratic nonlinear media," Phys. Rev. Lett. **108**, 113903 (2012).
21. R. Bekenstein and M. Segev, "Self-accelerating optical beams in highly nonlocal nonlinear media," Opt. Express **19**, 23706–23715 (2011).
22. I. Kaminer, R. Bekenstein, J. Nemirovsky, and M. Segev, "Nondiffracting accelerating wave packets of Maxwell's equations," Phys. Rev. Lett. **108**, 163901 (2012).
23. F. Courvoisier, A. Mathis, L. Froehly, R. Giust, L. Furfaro, P. A. Lacourt, M. Jacquot, and J. M. Dudley, "Sending femtosecond pulses in circles: highly nonparaxial accelerating beams," Opt. Lett. **37**, 1736–1738 (2012).
24. I. Kaminer, J. Nemirovsky, and M. Segev, "Self-accelerating self-trapped nonlinear beams of Maxwell's equations," Opt. Express **20**, 18827–18835 (2012).
25. P. Zhang, Y. Hu, D. Cannan, A. Salandrino, T. Li, R. Morandotti, X. Zhang, and Z. Chen, "Generation of linear and nonlinear nonparaxial accelerating beams," Opt. Lett. **37**, 2820–2822 (2012).
26. P. Aleahmad, M. A. Miri, M. S. Mills, I. Kaminer, M. Segev, and D. N. Christodoulides, "Fully vectorial accelerating diffraction-free Helmholtz beams," Phys. Rev. Lett. **109**, 203902 (2012).
27. P. Zhang, Y. Hu, T. Li, D. Cannan, X. Yin, R. Morandotti, Z. Chen, and X. Zhang, "Nonparaxial Mathieu and Weber accelerating beams," Phys. Rev. Lett. **109**, 193901 (2012).
28. M. A. Bandres and B. M. Rodríguez-Lara, "Nondiffracting accelerating waves: Weber waves and parabolic momentum," New J. Phys. **15**, 013054 (2013).
29. M. A. Bandres, M. A. Alonso, I. Kaminer, and M. Segev, "Three-dimensional accelerating electromagnetic waves," Opt. Express **21**, 13917–13929 (2013).
30. M. A. Bandres, I. Kaminer, M. S. Mills, B. M. Rodríguez-Lara, E. Greenfield, M. Segev, and D. N. Christodoulides, "Accelerating optical beams," Opt. Photon. News **24**(6), 30–37 (2013).
31. R. Penciu, V. Paltoglou, and N. K. Efremidis, "Closed-form expressions for nonparaxial accelerating beams with pre-engineered trajectories," Opt. Lett. **40**, 1444–1447 (2015).
32. A. Mathis, F. Courvoisier, R. Giust, L. Furfaro, M. Jacquot, L. Froehly, and J. M. Dudley, "Arbitrary nonparaxial accelerating periodic beams and spherical shaping of light," Opt. Lett. **38**, 2218–2220 (2013).
33. Z. Liu, Y. Zhang, Y. Zhang, P. Liang, J. Yang, and L. Yuan, "All-fiber self-accelerating Bessel-like beam generator and its application," Opt. Lett. **39**, 6185–6188 (2014).
34. C. Vetter, T. Eichelkraut, M. Ornigotti, and A. Szameit, "Generalized radially self-accelerating helicon beams," Phys. Rev. Lett. **113**, 183901 (2014).
35. I. D. Chremmos and N. K. Efremidis, "Nonparaxial accelerating Bessel-like beams," Phys. Rev. A **88**, 063816 (2013).
36. F. Oberhettinger, *Tables of Fourier Transforms and Fourier Transforms of Distributions* (Springer-Verlag, 1990).
37. M. Abramowitz and I. Stegun, *Handbook of Mathematical Functions* (Dover, 1972).
38. R. Schley, I. Kaminer, E. Greenfield, R. Bekenstein, Y. Lumer, and M. Segev, "Loss-proof self-accelerating beams and their use in non-paraxial manipulation of particles' trajectories," Nat. Commun. **5**, 5189 (2014).
39. Y. Li, C. Qiu, S. Xu, M. Ke, and Z. Liu, "Theoretical study of large-angle bending transport of microparticles by 2D acoustic half-Bessel beams," Sci. Rep. **5**, 13063 (2015).